Available online at www.sciencedirect.com

ScienceDirect

IFAC Papers Online CONFERENCE PAPER ARCHIVE

IFAC-PapersOnLine 49-7 (2016) 153–158

Control of incomplete separation in simulated moving bed chromatographic processes

Paul Suvarov*, Alain Vande Wouwer*,
Ju Weon Lee, Andreas Seidel-Morgensten**, Achim Kienle****

** Service d'Automatique, Université de Mons (UMONS), B-7000 Mons, Belgium (e-mail: Alain.VandeWouwer@umons.ac.be)*
*** Max-Planck-Institut für Dynamik komplexer technischer Systeme, D-39106 Magdeburg, Germany (e-mail:Kienle@mpi-magdeburg.mpg.de)*

Abstract: Simulated moving bed (SMB) is a continuous chromatographic process used for the separation of fluid mixtures. This paper presents a simple control strategy to handle incomplete separation, which requires tight control to achieve the desired purities. At first, a discrete-time nonlinear model is derived from wave theory, which will be the basis to estimate the position of the adsorption and desorption fronts. Four controllers are designed, two for the position of the concentration waves in zone 1 and 4, and two for the purities at the extract and raffinate outlets. The performance of the control strategy is evaluated with an experimental study of the separation of racemic Bicalutamide enantiomers in a 4 column-SMB.

Keywords: chromatography, process control, adaptive control, parameter estimation

1. INTRODUCTION

Simulated Moving Bed (SMB) chromatographic separation processes allow the continuous separation of binary mixtures. They were first used in large scale production by universal oil products (UOP) in the early 60's (Broughton and Gerhold, 1961). Following their successful application to hydrocarbon and sugar separation, the technology was improved and increasingly applied to the separation of high-added value chemicals and pharmaceuticals.

A schematic view of a typical SMB process is presented in figure 1. The inputs (feed mixture and solvent) and outputs (extract and raffinate) divide the system in four zones each containing one or more chromatographic columns, depending on the separation being performed. Pumps connected at each port determine the liquid phase flow rates in the zones.

The feed mixture is injected between zone 2 and 3. The adsorbent is chosen in such a way that the two components are adsorbed at different rates, allowing them to travel with different velocities. The less adsorbed component (A) is collected at the raffinate port and the more adsorbed one (B) at the extract port. In a total separation configuration, the separation of the two components is performed in zone 2 and 3, whereas zones 1 and 4 are dedicated to adsorbent regeneration and solvent recycling, respectively.

The liquid-solid counter-current movement can be obtained by rotating the columns containing the adsorbent in the opposite direction to the liquid phase flow, as shown in figure 1. A specific equilibrium between the velocities of the liquid and solid phases must be achieved so as to ensure that the separation occurs in a desired way. The corresponding operating points for total separation can be obtained using the triangle theory (Storti et al., 1993; Mazzotti et al., 1997).

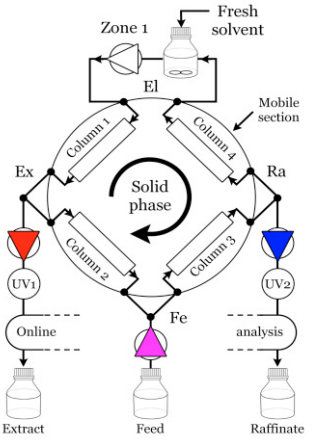

Figure 1. SMB configuration

Besides the selection of optimal operating conditions, the regulation of the process in order to reject potential disturbances has also attracted considerable attention, e.g. inferential PI controller (Schramm et al., 2003), the 'cycle to cycle' control concept based on model predictive control (Grossmann et al., 2008), (Erdem et al., 2005), (Song et al., 2006), (Engell and Toumi, 2005).

In (Fütterer, 2008; Suvarov et al., 2014), a simple adaptive control scheme has been proposed to achieve total separation. It is based on a discrete-time model of the front wave positions and on-line estimation of the optimal open-loop inputs to the plant to ensure total separation with maximum productivity. The resulting control scheme is extremely simple, combining feedforward actions (the estimated open-loop inputs) and feedback actions in the form of 4 proportional controllers regulating the position of the adsorption and desorption waves in their respective zones. Little prior knowledge about the adsorption properties

10.1016/j.ifacol.2016.07.232

(isotherm parameters) is required, and the controller appears as a self-optimizing strategy as it allows the concentration fronts to be moved in optimal locations.

In the present study, the control concept is extended to handle the case of incomplete separation. In contrast with the total separation case, the concentration wave fronts do not stay confined in a zone, but can cross the extract and raffinate outlets (which is logical since the purity is reduced). The control strategy consists of 2 wave position controllers in zone 1 and 4, and 2 purity controllers at the raffinate and extract outlets. The operation of this controller is illustrated by experimental results obtained with the separation of racemic Bicalutamide. The experiments presented in this paper were carried out at low concentrations where a decentralized control approach seems sufficient. For higher feed concentrations, the interaction between the control loops becomes significant, so that some decoupling or a centralized control approach would be required.

The paper is organized as follows. The next section describes the mass-balance partial differential equation (PDE) model of the SMB plant. In the third section, a discrete-time model of the location of the foot point of the concentration fronts is derived. This model is used in section 4 to design a simple adaptive control scheme, which is tested in an experimental case study in section 5. Conclusions and prospects are given in section 6.

2. SMB MODELING AND SIMULATION

For the typical SMB unit of figure 1, with 1:1:1:1 column configuration, a system of 16 mass balance PDEs (1-2) can be derived. The mass transfer between the two phases is represented by a **L**inear **D**riving **F**orce model (2).

$$\frac{\partial C_{i,j}}{\partial t} + F\frac{\partial q_{i,j}}{\partial t} + v_j \frac{\partial C_{i,j}}{\partial z} = D_j \frac{\partial^2 C_{i,j}}{\partial z^2}, \quad i = A,B; \;\; j = 1,...,4 \tag{1}$$

$$\frac{\partial q_{i,j}}{\partial t} = K_i (q_{i,j}^{eq} - q_{i,j}), \;\; D_j = \frac{Lv_j}{2N}, \;\; F = \frac{1-\varepsilon}{\varepsilon} \tag{2}$$

where $C_{i,j}$ and $q_{i,j}$ represent the concentrations of the two components in the liquid and solid phase, F is the phase ratio, ε is the column porosity, v_j is the speed of the liquid phase, D_j is the axial dispersion coefficient, K_i is the mass transfer coefficient, L is the length of a column, N is the number of theoretical plates, i identifies the component in the feed mixture and j the column.

The equilibrium between the two phases is described by a bi-Langmuir isotherm (3) for the racemic Bicalutamide separation (Kaemmerer et al., 2012).

$$q_i^{eq} = \frac{q_{s1,i} b_{1,i} C_i}{1 + b_{1,A} C_A + b_{1,B} C_B} + \frac{q_{s2,i} b_{2,i} C_i}{1 + b_{2,A} C_A + b_{2,B} C_B}, \;\; i = A,B \tag{3}$$

The initial slope of the isotherms correspond to the Henry coefficients given by:

$$H_i = q_{s1,i} b_{1,i} + q_{s2,i} b_{2,i}, \;\; i = A,B \tag{4}$$

Dirichlet boundary conditions are considered at the input of each column. For columns 2 and 4, these conditions simply express concentration continuity.

$$C_{i,j+1}(0,t) = C_{i,j}(L,t), \;\; i = A,B; \;\; j = 2,4 \tag{5}$$

while for columns 1 and 3, at the solvent or feed port, respectively, the conditions are:

$$C_{i,1}(0,t) = \frac{v_4 C_{i,4}(L,t)}{v_1}, \;\; i = A,B \tag{6}$$

$$C_{i,3}(0,t) = \frac{v_2 C_{i,2}(L,t) + v_{Fe} C_{i,Fe}}{v_3}, \;\; i = A,B \tag{7}$$

where $v_{1...4}$ are the liquid phase velocities in each zone, v_{Fe} and $C_{i,Fe}$ are the velocity and concentrations of the two components in the feed mixture injected.

At the output of each column, zero-dispersion and zero-adsorption conditions are expressed using a simple advection equation (Haag et al., 2001).

$$\frac{\partial C_{i,j}(L,t)}{\partial t} = -v_j \frac{\partial C_{i,j}(L,t)}{\partial z} \;\; i = A,B; \;\; j = 1,...,4 \tag{8}$$

The counter-current movement needed for the separation is obtained by rotating the columns in the opposite direction of the liquid phase while the boundary conditions are fixed, by one column length every cycle.

The SMB model is simulated using a method of lines approach with finite elements and quadratic basis functions for spatial discretization, and a stiff differential ordinary differential equation solver, as available in Matlab and the MatMol library (Vande Wouwer et al., 2014). A typical simulation result obtained with 16 elements per column is shown in figure 3 for the separation of racemic Bicalutamide (total separation with optimal productivity).

3. WAVE FRONT MODELING

In order to regulate the purities at the extract and raffinate outlets, the position of the concentration waves must be controlled by adjusting the external flow rates and the cycle duration T_{SW}.

In this section, a model describing the movement of concentration waves is derived and used to set-up a one-cycle ahead predictor. UV detectors are assumed available at the extract and raffinate outlets, as shown in figure 1.

The foot point of a concentration wave is located at the intersection of the wave profile with a threshold chosen in accordance with the UV detector sensitivity and the presence of noise, as depicted in figure 2.

It is assumed that the velocity of the wave v_w is constant during one cycle and is directly proportional to the flow-rate in the corresponding zone.

The traveling time of the wave from its initial position to the UV detector can be determined from the measurements, and in turn the position of the wave (figure 3 and equations 9-10). This value is normalized with respect to the duration of the

cycle, and is referred to as the normalized retention time τ .

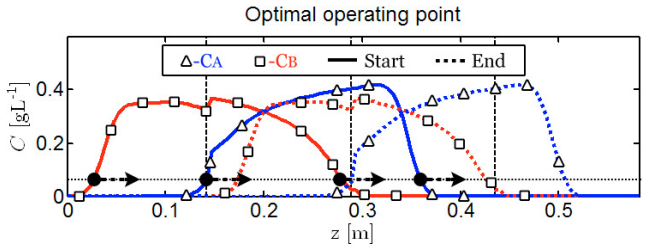

Figure 2. Concentration profiles inside the SMB at cyclic steady state (optimal separation point for racemic Bicalutamide), and threshold used to detect the foot-points of the wave profiles.

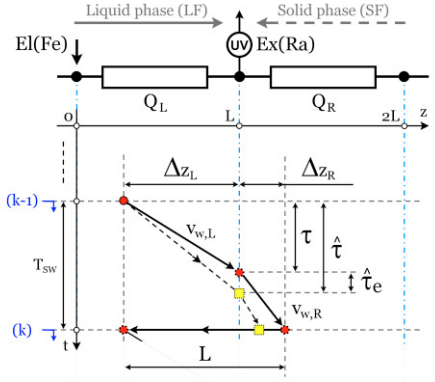

Figure 3. Foot-point movement during one cycle. Round dot represents the actual foot-point location while the squared one is the estimated location.

$$\Delta z_L(k-1) = v_{w,L}(k-1)T_{SW}(k-1)\tau(k-1) \tag{9}$$

$$\Delta z_R(k-1) = v_{w,R}(k-1)T_{SW}(k-1)\big(1-\tau(k-1)\big) \tag{10}$$

When commutation occurs, the wave front is shifted by one column length.

$$\Delta z_L(k) = L - \Delta z_R(k-1) \tag{11}$$

The wave velocity is assumed to be proportional to the fluid flow rate at the left and right side of the UV detector, and inversely proportional to a θ parameter which is dependent on the adsorbent properties. All columns are assumed identical, therefore the θ parameter do not vary from column to column at the given flow-rate condition.

$$v_{w,i}(k) = Q_i(k)\frac{L}{\theta}, \quad i = L,R \tag{12}$$

For linear isotherms, the parameters can be obtained from the characteristic speed of the waves. Four θ parameters are required for a 4 zone SMB system.

$$v_{ci,j} = \frac{F+1}{A}\frac{Q_j}{H_i F+1} = \frac{L}{\theta_j}Q_j; \; i = A,B; \quad j = 1,\ldots,4 \tag{13}$$

$$\theta_1 = \theta_3 = \frac{AL(H_B F+1)}{F+1} \tag{14}$$

$$\theta_2 = \theta_4 = \frac{AL(H_A F+1)}{F+1} \tag{15}$$

where A is the cross-sectional area of the column.

For nonlinear isotherms, such as (3), equations (14-15) can be extended by considering the optimal flow-rate ratios m_j determined using the triangle theory (generalized to the isotherms under consideration).

$$\theta_j = \frac{AL(m_j F+1)}{F+1}, \quad j = 1,\ldots,4 \tag{16}$$

A one-cycle ahead predictor of the retention time is given by (17 - 18).

$$\hat{\tau}_j(k) = \frac{\theta_j - Q_R(k-1)T_{SW}(k-1)\big(1-\tau_j(k-1)\big)}{Q_L(k)T_{SW}(k)}, \quad j = 1,3 \tag{17}$$

$$\hat{\tau}_j(k) = 1 - \frac{\theta_j + Q_R(k-1)T_{SW}(k-1)\tau_j(k-1)}{Q_L(k)T_{SW}(k)}, \quad j = 2,4 \tag{18}$$

4. PARAMETER ESTIMATION AND CONTROL

The estimated parameters $\hat{\theta}_j$ can be seen as the optimal open loop inputs to the process that result in total separation and regeneration.

$$\hat{\theta}_j(k-1) = \hat{Q}_j(k-1)\hat{T}_{SW}(k-1), \quad j = 1,\ldots,4 \tag{19}$$

Changes in time of the adsorption properties of the columns are tracked using a parameter estimation strategy. They have indeed a visible effect on the measurements as illustrated in figure 3. The errors between the measured normalized retention time (round red dot) and the estimated normalized retention time given by the foot-point model (squared yellow dot) gives the estimated retention time error $\hat{\tau}_{e,j}(k)$.

$$\theta_{err,j}(k-1) = Q_j(k-1)T_{SW}(k-1)\hat{\tau}_{e,j}(k-1) \tag{20}$$

A parameter estimation scheme can be designed accordingly for each concentration wave (see figure 4)

$$\hat{\theta}_j(k) = \hat{\theta}_j(k-1) + (1-K_\theta)\theta_{err,j}(k-1), \; 0 \le K_\theta \le 1 \tag{21}$$

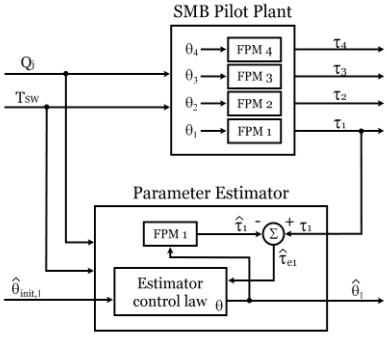

Figure 4. Parameter estimation scheme.

Initial parameters $\hat{\theta}_{Init,j}$ are determined using equations (14-15).

To face disturbances, 4 PI feedback controllers are introduced. The controller outputs are the cyclic volumetric flow-rates $\bar{Q}_j(k) = Q_j(k)T_{SW}(k)$.

$$\bar{Q}_1(k) = \hat{\theta}_1(k)\{1+[1-\tau_{Ref,1}(k-1)]\} \left(1 - K_{P,1}e_1(k) - K_{I,1}\sum_{p=0}^{k}\frac{e_1(p)+e_1(p-1)}{2}\right) \quad (22)$$

$$\bar{Q}_2(k) = \hat{\theta}_2(k)P_{Ref,Ex}(k-2) \left(1 - K_{P,2}e_2(k) - K_{I,2}\sum_{p=0}^{k}\frac{e_2(p)+e_2(p-1)}{2}\right) \quad (23)$$

$$\bar{Q}_3(k) = \hat{\theta}_3(k)\{1+[1-P_{Ref,Ra}(k-2)]\} \left(1 - K_{P,3}e_3(k) - K_{I,3}\sum_{p=0}^{k}\frac{e_3(p)+e_3(p-1)}{2}\right) \quad (24)$$

$$\bar{Q}_4(k) = \hat{\theta}_4(k)\tau_{Ref,4}(k-1) \left(1 - K_{P,4}e_4(k) - K_{I,4}\sum_{p=0}^{k}\frac{e_4(p)+e_4(p-1)}{2}\right) \quad (25)$$

As the feed flow-rate is imposed by the production requirements, the cycle duration is adapted accordingly.

$$T_{SW}(k) = \frac{\bar{Q}_3(k) - \bar{Q}_2(k)}{Q_{Fe}^*} \quad (26)$$

The internal/external flow rates are then computed:

$$Q_j = \frac{\bar{Q}_j(k)}{T_{SW}(k)} \quad (27)$$

$$Q_{El} = Q_1 - Q_4;\ Q_{Ex} = Q_1 - Q_2;\ Q_{Ra} = Q_3 - Q_4 \quad (28)$$

The manipulated variables are therefore the 4 external flow-rates and the cycle duration.

It is also possible to incorporate constraints on the maximum flow-rates. If one of the following inequality constraints is violated, the cycle duration is determined from the corresponding maximum flow-rate. In this case it is necessary to accept a variation of the feed flow-rate.

$$\frac{\bar{Q}_1(k)}{Q_{1,\max}} \le T_{SW}(k), \qquad \frac{\bar{Q}_1(k) - \bar{Q}_2(k)}{Q_{Ex,\max}} \le T_{SW}(k) \quad (29)$$

$$\frac{\bar{Q}_3(k) - \bar{Q}_2(k)}{Q_{Fe,\max}} \le T_{SW}(k), \quad \frac{\bar{Q}_3(k) - \bar{Q}_4(k)}{Q_{Ra,\max}} \le T_{SW}(k) \quad (30)$$

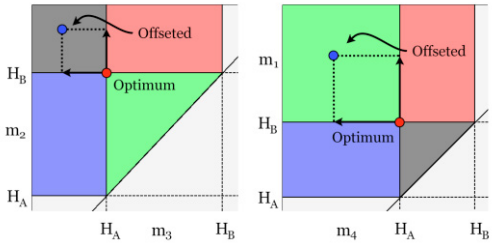

Figure 5. Computation of the operating point in the reduced purity region (left) and total regeneration (right).

In the expressions (22-25), the feedforward actions are computed from the total separation optimal inputs (θ_j), with a multiplicative factor depending on the set-points aimed at imposing the operating point into the reduced purity zone, see figure 5 illustrating the separation of racemic Bicalutamide at low concentration (nearly linear isotherms defined by the Henry coefficients (4)). The nonlinearity of the isotherms usually increases with the concentration of the feed mixture, and the separation regions will change accordingly.

The control strategy is summarized in figure 6. The Labview SMB interface, receives measurement information at the beginning of each cycle, computes the necessary control action, limits the outputs to the specified limits and sends the new control action. During the execution of each cycle, all outputs are fixed.

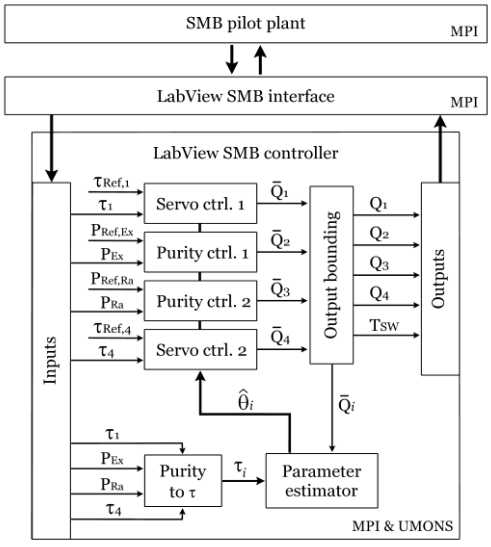

Figure 6. Control structure

5. SEPARATION OF RACEMIC BICALUTAMIDE

A racemic mixture of Bicalutamide, a drug substance used in the treatment of prostate cancer (it is the active pharmaceutical ingredient in AstraZeneca product CASODEX), is separated using a 4-column Knauer SMB plant with rotative valve, as illustrated in figure 1. The column are packed with a stationary phase Chiralpak AD (Daicel Chemical Industries Ltd.). The details of the technical set-up can be found in (Kaemmerer et al., 2012).

Figure 7-8 show simulation results of the open-loop operation of the plant in a sequence of 3 situations: (a) total separation with optimal productivity until cycle 34 (corresponding to the spatial concentration profiles in figure 3) (b) reduced purities until cycle 69 (c) a sharp disturbance of -20% in the Henry coefficients affecting the separation regions, and in turn, a significant change in the purities.

These simulation results clearly motivate the use of feedback control, which is now tested in real-life application. Important parameter values are given in Tables 1-3.

First, the pilot plant is operated in open-loop (from cycle 1 to 8). During this interval, the parameter estimator is active and converges (see Figure 9). At cycle 9, the controllers are switched on with set-points close to the actual measurements, in order to minimize start-up bumps. The plant then operates in closed-loop for several cycles at total separation (from cycle 9 to 49). The purity set-points are then changed from 100% to 80% at both outlets (cycles 50 to 78). The purities

and their set-points are illustrated in figure 10.

The set-points for the regeneration waves in zones 1 and 4 are set to 0.6. Figure 11 shows the evolution of the normalized retention times obtained from the UV measurements and their estimates given by the foot-point models.

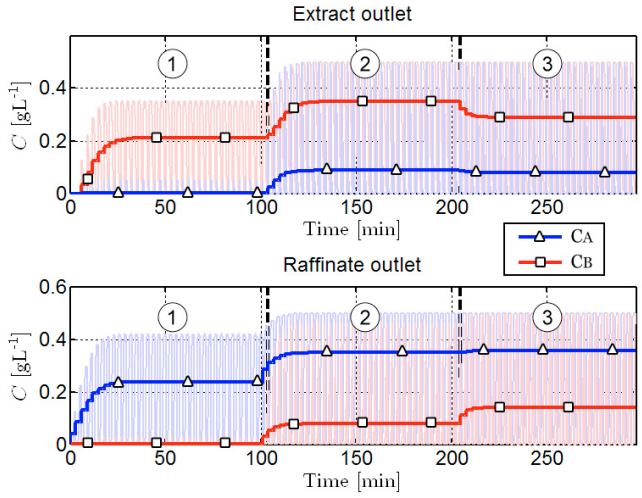

Figure 7. Time evolution of outlet concentrations following a change of operating point (from total separation to reduced purities), and a disturbance of the Henry coefficients.

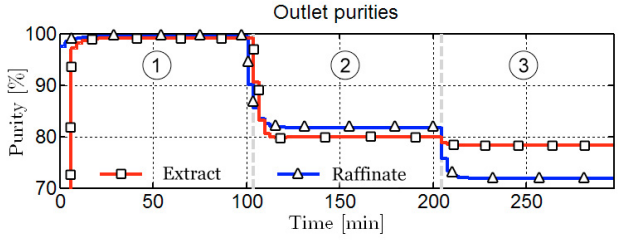

Figure 8. Time evolution of the purities following a change of operating point (from total separation to reduced purities), and a disturbance of the Henry coefficients.

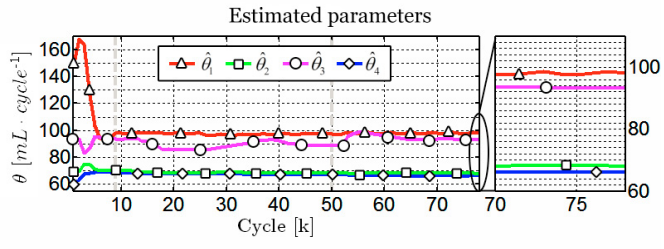

Figure 9. Experimental results: Convergence of the parameter estimates.

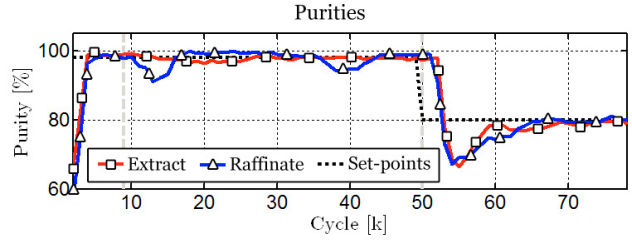

Figure 10. Experimental results: time evolution of the purities following a change of operating point from 100% to 80%.

The initial operating point is set relatively close to the tip of the triangle (optimal total separation point). Indeed, Figure 9 shows that the estimated $\hat{\theta}$ parameters for zone 2 and 3 remain at the same level. After the change in the purity set-points (from cycle 50 on), $\hat{\theta}_3$ increases slightly suggesting that the separation region has been slightly modified. Column 3 is the most loaded column, and isotherm nonlinearities are more apparent in this column.

During the first two parts of the experiment, the cycle duration varies around the initial value mostly because the feed flow-rate is already at the imposed value.

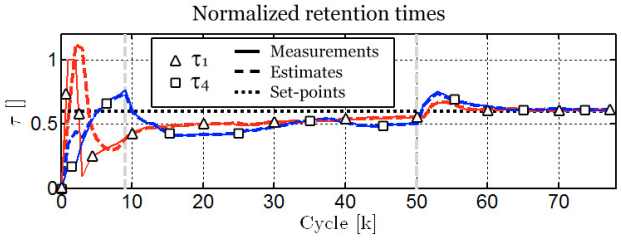

Figure 11. Experimental results: time evolution of the normalized residence times.

When the purity set-points are changed, the flow-rate in zone 2 is decreased considerably. Since the feed flow-rate is imposed all the other flow-rates are decreased. The only way to achieve the cyclic volumetric flow-rates required by the controllers is therefore to increase the cycle duration. These effects are seen in the trajectories of the manipulated variables illustrated in figure 12-13.

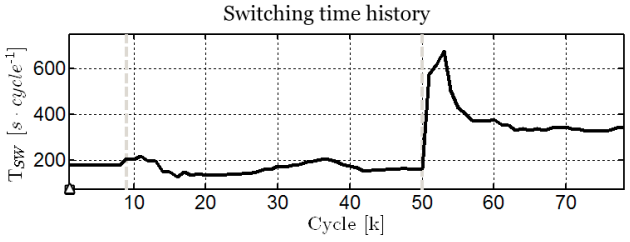

Figure 12. Experimental results: time evolution of the switching period

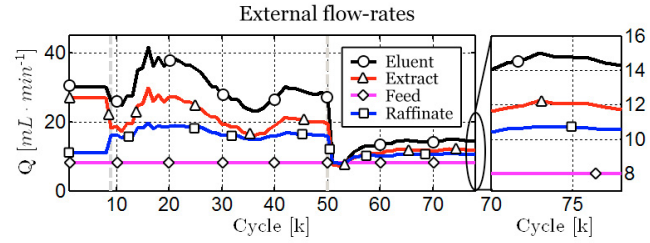

Figure 13. Experimental results: time evolution of the flow rates.

The manipulated variables and the estimates can be translated to the flow-ratio domain using (31).

Figure 14 shows that $m_{2,3}$ follow closely their estimates until cycle 49. The small variation in the outlet purities are correlated to the actions of the controllers regulating the regeneration front-waves. After the purity set-points are

changed, and controllers are close to cyclic steady state, an offset between $m_{2,3}$ and their estimates is observed. This indicates operation outside the total separation region.

$$m_j(k) = \frac{Q_j T_{SW} - \varepsilon AL}{(1-\varepsilon)AL}; \quad \hat{m}_j(k) = \frac{\hat{\theta}_j - \varepsilon AL}{(1-\varepsilon)AL} \tag{31}$$

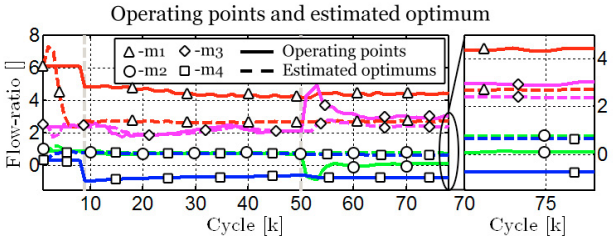

Figure 14. Experimental results: time evolution of the operating points (continuous lines) and the estimated optimum operating points indicated by the parameter estimator (dashed lines).

Table 1. Simulation and experimental common parameters

Parameter	Value	Parameter	Value
$C_{A.Fe}(g \cdot L^{-1})$	0.5	$C_{B.Fe}(g \cdot L^{-1})$	0.5
H_A	0.5360	H_B	3.8071
$K_A(s^{-1})$	0.5	$K_B(s^{-1})$	0.5
$L\ (m)$	0.1467	$D\ (m)$	0.0250
ε	0.783	N	100

Table 2. Simulation and experimental operating points

Param	Value	Param.	Value
m_{Sim1}	$[4.062 \quad 0.617 \quad 2.083 \quad -0.974]$	$T_{SW}(s)$	178
$m_{Sim2,3}$	$[4.062 \quad -0.447 \quad 3.385 \quad -0.97]$	$T_{SW}(s)$	178
m_{Exp}	$[6.091 \quad 0.857 \quad 2.379 \quad 0.335]$	$T_{SW}(s)$	178

Table 3.Controller and estimator parameters

Param.	Value	Param.	Value	Param.	Value
K_{P1}	0.15	K_{I1}	0.1	K_θ	0.75
K_{P2}	0.8	K_{I2}	0.07	$Q^*_{Fe}\left(mL \cdot min^{-1}\right)$	8
K_{P3}	0.8	K_{I3}	0.07	$Th(AU)$	100
K_{P4}	0.15	K_{I4}	0.1		

6. CONCLUSION

In this work, a simple adaptive control strategy is presented to regulate incomplete separation in SMB chromatographic processes. The efficiency of this strategy is demonstrated experimentally with the separation of a racemic mixture of Bicalutamide. The controller appears extremely robust and allows the on-line identification of the optimal operating points even with very little knowledge of the adsorption characteristics. The price to pay is however the availability of UV detectors and of an on-line analysis system at the extract and raffinate outlets.

REFERENCES

Engell, S. and Toumi, A. (2005). *Optimisation and control of chromatography*, Computers and Chemical Engineering 29(6), p. 1243–1252.

Erdem, G., Abel, S., Amanullah, M., Morari, M., Mazzotti, M. and Morbidelli, M. (2005). *Automatic control of simulated moving beds — experimental verification*, Adsorption 11(1), p. 573–577.

Fütterer, M. (2008). *An Adaptive Control Concept for Simulated Moving Bed Plants in Case of Complete Separation*, Chemical Engineering and Technology 31(10), p. 1438–1444.

Grossmann, C., Erdem, G., Morari, M., Amanullah, M., Mazzotti, M. and Morbidelli, M. (2008). *'Cycle to cycle' Optimizing Control of Simulated Moving Beds*, AIChE Journal 54(1), p. 194-208.

Kaemmerer, H., Horvath, Z., Lee, J.W., J., Kaspereit, M., Arnell, R., Hedberg, M., Herschend, B., Jones M.J., Larson, K., Lorenz H., and Seidel-Morgensten, A. (2012). *Separation of Racemic Bicalutamide by an Optimized Combination of Continuous Chromatography and Selective Crystallization, Org*. Process Res. Dev.16, p. 331–342.

Mazzotti, M., Storti, G. and Morbidelli, M. (1997). *Optimal operation of simulated moving bed units for nonlinear chromatographic separations*, Journal of Chromatography A 769(1), p. 3–24.

Schramm, H., Gröner, S. and Kienle, A. (2003). *Optimal operation of simulated moving bed chromatographic processes by means of simple feedback control*, Journal of Chromatography A 1006(1–2), p. 3–13.

Schramm, H., Kaspereit, M., Kienle, A. and Seidel-Morgenstern, A. (2003). *Simulated moving bed process with cyclic modulation of the feed concentration*, Journal of Chromatography A 1006, p. 77–86.

Schramm, H., Kienle, A., Kaspereit, M., and Seidel-Morgenstern, A. (2003). *Improved operation of simulated moving bed processes through cyclic modulation of feed flow and feed concentration*, Chemical Engineering Science 58(23-24), p. 5217–5227.

Song, I.H., Lee, S.B., Rhee, H.K. and Mazzotti, M. (2006). *Optimization-based predictive control of a simulated moving bed process using an identified model*, Chemical Engineering Science 61(18), p. 5179–6165.

Suvarov, P., Kienle, A., Nobre Goncalves, C., De Weireld, G. and Vande Wouwer, A. (2014). *Cycle to cycle adaptive control of simulated moving bed chromatographic separation processes*, Journal of Process Control 24 (2014), 357–367.

Storti, G., Mazzotti, M., Morbidelli, M. and Carrà, S. (1993). *Robust design of binary countercurrent adsorption separation processes*, AIChE Journal 39(3, p. 471–492.

Vande Wouwer, A., Saucez, P. and Vilas, C. (2014). *Simulation of ODE/PDE Models with MATLAB®, OCTAVE and SCILAB*, Springer.